

Magnetic excitations in the three-dimensional dilute antiferromagnet $\text{Fe}_x\text{Zn}_{1-x}\text{F}_2$

This article has been downloaded from IOPscience. Please scroll down to see the full text article.

2002 J. Phys.: Condens. Matter 14 1307

(<http://iopscience.iop.org/0953-8984/14/6/317>)

View [the table of contents for this issue](#), or go to the [journal homepage](#) for more

Download details:

IP Address: 171.66.16.27

The article was downloaded on 17/05/2010 at 06:08

Please note that [terms and conditions apply](#).

Magnetic excitations in the three-dimensional dilute antiferromagnet $\text{Fe}_x\text{Zn}_{1-x}\text{F}_2$

Junko Satooka^{1,4}, Koichi Katsumata^{1,2} and David P Belanger³

¹ RIKEN (The Institute of Physical and Chemical Research), Wako, Saitama 351-0198, Japan

² RIKEN Harima Institute, Mikazuki, Sayo, Hyogo 679-5148, Japan

³ Department of Physics, University of California, Santa Cruz, CA 95064, USA

E-mail: satooka@ynu.ac.jp

Received 25 September 2001

Published 1 February 2002

Online at stacks.iop.org/JPhysCM/14/1307

Abstract

Fourier-transform infrared spectroscopy measurements have been performed on single crystals of the three-dimensional dilute antiferromagnet $\text{Fe}_x\text{Zn}_{1-x}\text{F}_2$ with $x = 0.99$ – 0.58 in the far-infrared (FIR) region. A magnetic excitation spectrum is observed below the transition temperature. The spectra are analysed, taking into account the ligand field and the local exchange interaction probabilities with $J_1 \sim J_3$; $|J_1|, |J_3| \ll |J_2|$, where J_1 , J_2 , and J_3 are the nearest-neighbour, second-nearest-neighbour, and third-nearest-neighbour exchange interaction constants, respectively. The concentration dependence of the FIR spectra at low temperature is qualitatively well reproduced by our analysis.

1. Introduction

The dilute antiferromagnet $\text{Fe}_x\text{Zn}_{1-x}\text{F}_2$ has been studied extensively over the last two decades. In the concentrated region with $x > 0.4$, $\text{Fe}_x\text{Zn}_{1-x}\text{F}_2$ is an ideal example of the random-exchange Ising model without an applied field, and it becomes a prototypical example of the random-field Ising model when the field is applied along the spin easy axis [1]. Near to and below the percolation threshold $x_p \sim 0.246$ [2, 3], $\text{Fe}_x\text{Zn}_{1-x}\text{F}_2$ shows a cluster-glass behaviour [4–6]. Paduani *et al* [7] have investigated the magnetic excitations in $\text{Fe}_x\text{Zn}_{1-x}\text{F}_2$ using inelastic neutron scattering techniques and have reported that the spectrum obtained at a low temperature can be reproduced with three Gaussian peaks. No theoretical explanation has been given for this. In order to clarify the nature of the magnetic excitations in $\text{Fe}_x\text{Zn}_{1-x}\text{F}_2$, we have investigated the far-infrared (FIR) spectra of $\text{Fe}_x\text{Zn}_{1-x}\text{F}_2$ using a Fourier-transform infrared (FTIR) spectrophotometer with high resolution in zero field and have attempted to understand the results within the context of a molecular field model.

⁴ Present address: Yokohama National University, Hodogaya, Yokohama, Kanagawa 240-8501, Japan.

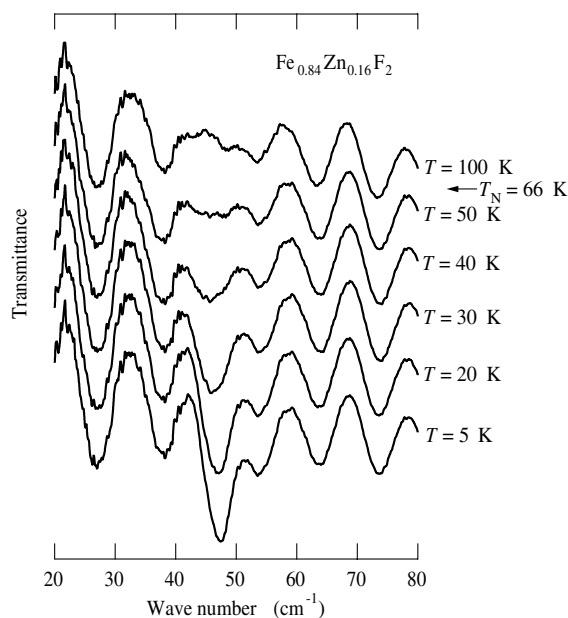


Figure 1. The measured temperature dependence of the FIR spectrum of $\text{Fe}_{0.84}\text{Zn}_{0.16}\text{F}_2$.

2. Experimental details

The single crystals of $\text{Fe}_x\text{Zn}_{1-x}\text{F}_2$ were grown⁵ using the Bridgman method. The platelets were polished to form a wedge in order to avoid interference between the light reflected from the upper plane and that from the lower plane of the sample. The strain at the surfaces of the sample, due to polishing, was removed by etching it in a 70 °C HCl solution for 1 min. The transition temperatures are $T_N = 78, 72, 66, 54,$ and 45 K for $x = 0.99, 0.91, 0.84, 0.68,$ and $0.58,$ respectively. The FIR spectra were measured with a bandwidth resolution of 0.1 cm^{-1} using a FTIR spectrophotometer made by the Bruker company, Germany. We used a high-pressure Hg lamp as a light source, a Mylar film with $23 \mu\text{m}$ thickness as a beamsplitter, and a Si bolometer as a detector. The temperature, T , of the sample was controlled using a helium cryostat from Oxford Instruments, UK.

3. Experimental results

The T -dependence of the FIR spectra of $\text{Fe}_{0.84}\text{Zn}_{0.16}\text{F}_2$ is shown in figure 1 as an example. The large oscillation is clear over the entire wavenumber range at any temperature. The absorption from about 30 to 60 cm^{-1} depends strongly on the temperature, increasing with decreasing T . Since it is striking even in the spectrum at $T = 100 \text{ K} \gg T_N$, we identify the oscillation as an interference effect. The spectrum at each T is interpreted as a superposition of the magnetic component which lies from about 30 to 60 cm^{-1} and the harmonic component occurring over the entire wavenumber range. In order to make the magnetic component stand out, we define the relative transmittance: $\text{transmittance}(T) - \text{transmittance}(T = 100 \text{ K})$. The T -dependence of the relative transmittance of $\text{Fe}_{0.84}\text{Zn}_{0.16}\text{F}_2$ is shown in figure 2. The oscillation in the relative transmittance is smaller than that in the raw transmittance shown in figure 1, but it still remains because the interference itself depends on T . We subtract a harmonic component from the

⁵ The crystals were grown at the University of California, Santa Barbara, by N Nighman.

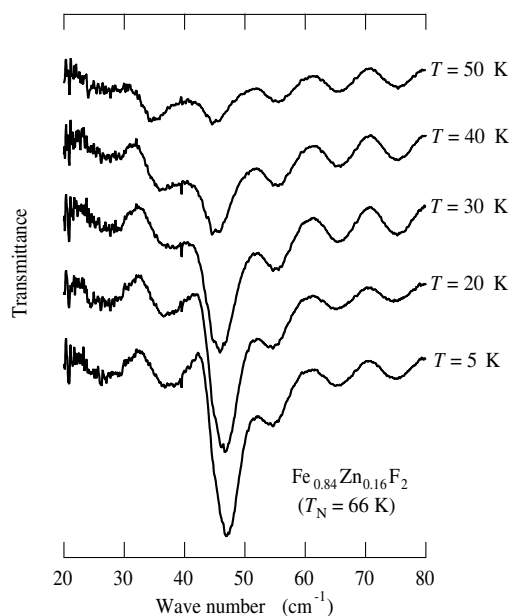


Figure 2. The temperature dependence of the relative transmittance; $\text{transmittance}(T) - \text{transmittance}(T = 100 \text{ K})$, of $\text{Fe}_{0.84}\text{Zn}_{0.16}\text{F}_2$.

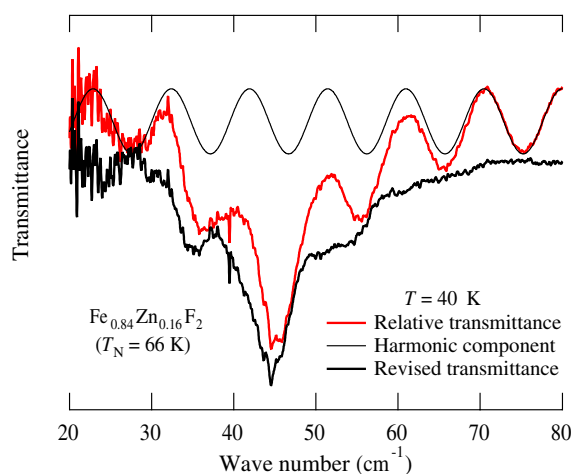


Figure 3. The revised FIR spectrum data for $\text{Fe}_{0.84}\text{Zn}_{0.16}\text{F}_2$ at $T = 40 \text{ K}$. On subtraction of the harmonic component from the relative transmittance, we get the revised transmittance, which clearly shows the magnetic contributions.

relative transmittance to get the revised transmittance, which yields the magnetic behaviour. An example of the subtraction at 40 K is shown in figure 3. The T -dependence of the revised transmittance of $\text{Fe}_{0.84}\text{Zn}_{0.16}\text{F}_2$ is shown in figure 4. The main broad absorption curve becomes broader and its position shifts gradually to lower energy as T increases below T_N . Two smaller satellite peaks are visible at all temperatures. The higher-energy one becomes broader as T increases, while the lower-energy one becomes sharper. Above T_N , no absorption is observed. This T -dependence of the FIR spectra is found to be common to all the samples investigated.

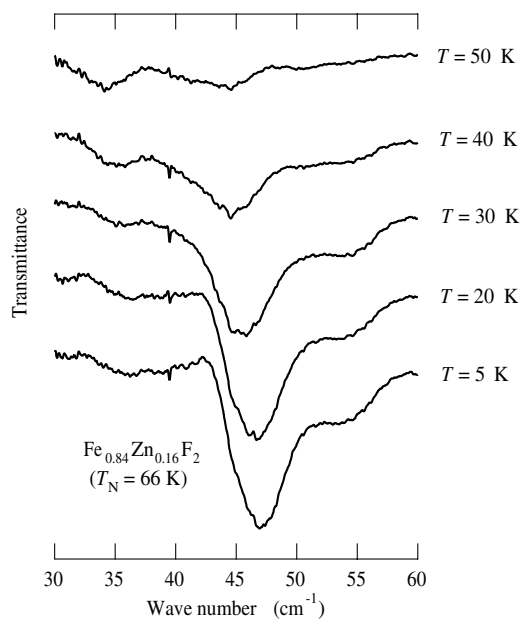


Figure 4. The temperature dependence of the revised transmittance of $\text{Fe}_{0.84}\text{Zn}_{0.16}\text{F}_2$.

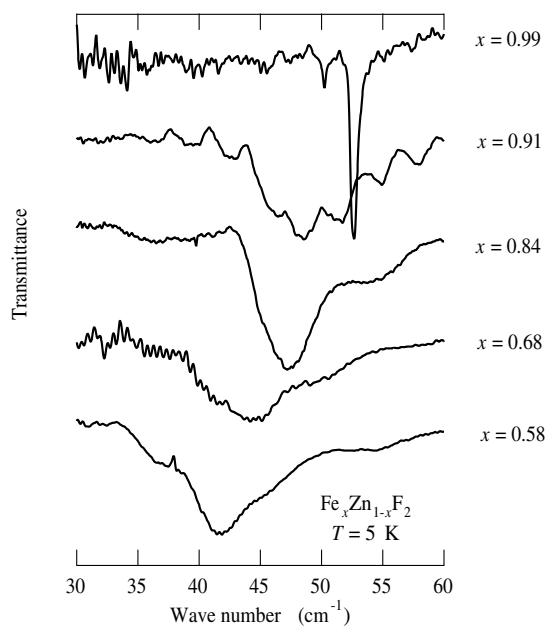


Figure 5. The concentration dependence of the revised transmittance of $\text{Fe}_x\text{Zn}_{1-x}\text{F}_2$ at $T = 5$ K.

The concentration dependence of the FIR spectrum of $\text{Fe}_x\text{Zn}_{1-x}\text{F}_2$ at 5 K is shown in figure 5. A very sharp absorption at 52.6 cm^{-1} is observed for $\text{Fe}_{0.99}\text{Zn}_{0.01}\text{F}_2$. The frequency of this absorption is in very good agreement with that of the antiferromagnetic resonance in FeF_2 ($52.7 \pm 0.2\text{ cm}^{-1}$) reported by Ohlman and Tinkham [8]. However, there is a small absorption

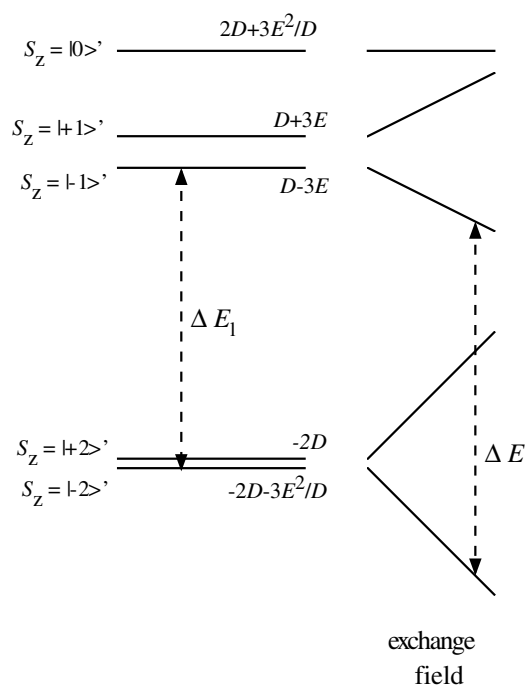


Figure 6. A schematic diagram of the splitting of the ion energy levels of the low-lying spin manifold for the rutile structure for a free Fe^{2+} ion.

in the spectrum of $\text{Fe}_{0.99}\text{Zn}_{0.01}\text{F}_2$ near 50 cm^{-1} which is not observed in the pure system. The absorption curve of $\text{Fe}_{0.91}\text{Zn}_{0.09}\text{F}_2$ is much broader than that of $\text{Fe}_{0.99}\text{Zn}_{0.01}\text{F}_2$. The oscillation in the spectrum of $\text{Fe}_{0.91}\text{Zn}_{0.09}\text{F}_2$ is considered to be an interference effect because this platelet is thicker than the others. With increasing dilution, the absorption curve becomes broader and its position shifts to lower energy. The FIR spectrum of $\text{Fe}_{0.58}\text{Zn}_{0.42}\text{F}_2$ is consistent with the $q = 0$ spectrum of $\text{Fe}_{0.59}\text{Zn}_{0.41}\text{F}_2$ measured by means of neutron scattering [7], except for the small lower-energy peak in the FIR spectrum.

4. Discussion and conclusions

To analyse the FIR spectra of $\text{Fe}_x\text{Zn}_{1-x}\text{F}_2$, we approximate the magnetic excitations in this system as single-ion ones, taking the exchange interactions between Fe^{2+} spins into account in the form of a molecular field. This should be a good approximation since the results of the magnetization measurements made on $\text{Fe}_x\text{Zn}_{1-x}\text{F}_2$ were successfully explained on the basis of a localized spin-flip model [9]. The non-diluted compound FeF_2 has the rutile-type crystal structure $D_{4h}^{14}-P4/mnm$ [10, 11]. The Fe^{2+} free ion has a $3d^6$ configuration and the ground state is 5D . Each Fe^{2+} ion is surrounded by six F^- ions forming an octahedron. The orbital state of the high-spin Fe^{2+} ion in an octahedral environment is split into the doublet 5E and the triplet 5T_2 by the cubic field: 5T_2 is the ground state and 5E is lifted up by some $10\,000\text{ cm}^{-1}$. The rhombic field removes all the orbital degeneracy of 5T_2 : A_{1g} is the ground state separated from B_{1g} and B_{2g} by ~ 1115 and $\sim 2400\text{ cm}^{-1}$ respectively [12]. Spin-orbit effects are adequately treated by perturbation methods, the effective Hamiltonian pertaining to the lowest orbital state of a single Fe^{2+} ion being

$$\mathcal{H} = -D\{S_z^2 - S(S+1)/3\} + E(S_x^2 - S_y^2) \quad (1)$$

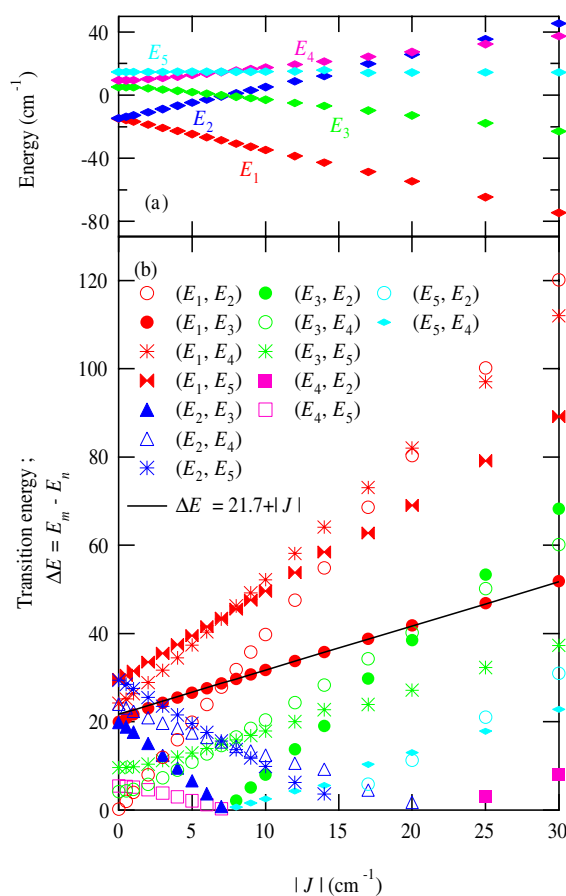


Figure 7. (a) The eigenvalues of energy and (b) the transition energy as a function of J . The solid line in (b) is the fitted line for the energy of the transition from E_1 to E_3 .

where z is taken parallel to the crystalline c -axis and D and E are the uniaxial and orthorhombic anisotropy constants. The schematic splitting of a free- Fe^{2+} -ion energy levels of the low-lying spin manifold for the rutile structure is shown in figure 6. As is seen from figure 4, the absorption intensities of the main broad peak and the higher-energy satellite peak decrease with increasing T . This indicates that the signal originates in the transition from the ground state. Tinkham [13] estimated that $D = 7.3 (\pm 0.7) \text{ cm}^{-1}$ and $E = 0.70 (\pm 0.04) \text{ cm}^{-1}$ from the analysis of the paramagnetic resonance of Fe^{2+} in ZnF_2 . Guggenheim *et al* [14] estimated $D = 6.46 (+0.29, -0.10) \text{ cm}^{-1}$ from inelastic neutron scattering results for FeF_2 .

The situation with an exchange interaction strength J is written as

$$\mathcal{H} = -D\{S_z^2 - S(S+1)/3\} + E(S_x^2 - S_y^2) - JS_z. \quad (2)$$

The eigenenergies obtained with $D = 7.3 \text{ cm}^{-1}$ and $E = 0.70 \text{ cm}^{-1}$ [13] are plotted in figure 7(a) as a function of $|J|$. They are labelled as E_1, E_2, \dots, E_5 , as shown in the figure. The energy of the transition from the state n to the higher state m , $\Delta E = E_m - E_n$, changes with $|J|$ as shown in figure 7(b). The probability of the transition is proportional to the product of two components. One is the difference in thermal population between the n -state and the m -state, $P_n - P_m$. The other is the square of the quantum-mechanical matrix element of S_x connecting

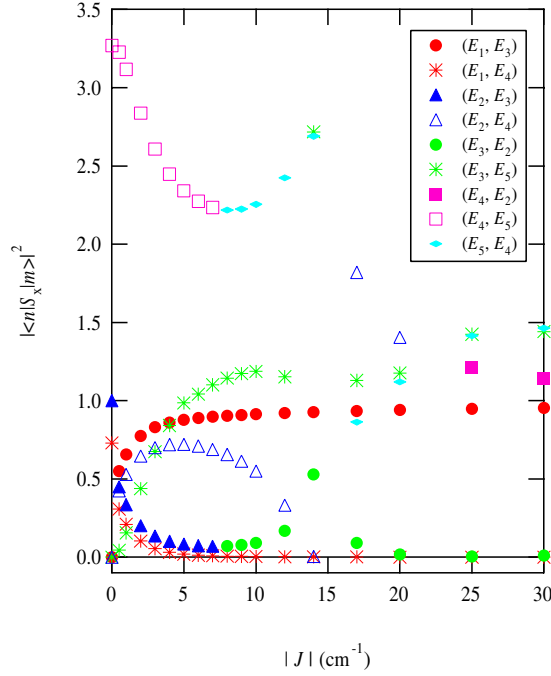


Figure 8. The values of $\langle n|S_x|m\rangle^2$ as a function of $|J|$. The notation (E_n, E_m) indicates the transition from state n to m .

states n and m , $\langle n|S_x|m\rangle^2$. The values of $\langle n|S_x|m\rangle^2$ are shown in figure 8 as a function of $|J|$. The thermal populations of each energy level at $T = 5$ K are shown in figure 9(a). So the probabilities of each transition that can occur at 5 K change with $|J|$ as shown in figure 9(b). This calculation clarifies that the transition from E_1 to E_3 is overwhelmingly dominant at 5 K. The energy of the transition between E_1 and E_3 depends almost linearly on $|J|$, as shown in figure 7(b). Therefore, the excitation energy for the transition at 5 K can be simplified to

$$\Delta E = \Delta E_l + |J| \quad (3)$$

where ΔE_l is a ligand field. ΔE and ΔE_l are shown schematically in figure 6 by dotted lines.

The probability, $p(i, n_i)$ that n_i magnetic ions occupy the z_i i th-nearest-neighbour sites is given by $[z_i!/(n_i!(z_i - n_i)!)]x^{n_i}(1 - x)^{z_i - n_i}$, with $i > 0$ and where x is the concentration of the magnetic ion. The sum of the local exchange interaction, $J(n_i) = J(n_1, n_2, \dots)$, and the probability that $J(n_i)$ is operative, $P(n_i) = P(n_1, n_2, \dots)$, are described as $J(n_i) = \sum_i J_i n_i$ and $P(n_i) = \prod_i p(i, n_i)$, respectively, where J_i describes the exchange interaction with the i th nearest neighbour. In the calculation, we consider the exchange interactions up to the third-nearest neighbours. The values of the parameters used are as follows: $J_1 = +0.048 \text{ cm}^{-1}$, $J_2 = -3.64 \text{ cm}^{-1}$, $J_3 = -0.194 \text{ cm}^{-1}$ [15], $z_1 = 2$, $z_2 = 8$, and $z_3 = 4$. The concentration dependence of the distribution of the local exchange interaction, $P_J(|J|, x)$, in $\text{Fe}_x\text{Zn}_{1-x}\text{F}_2$ is shown in figure 10. Taking into account the intrinsic linewidth of the experimental spectrum, we calculate the spectrum by replacing $|J|$ in equation (3) by a Gaussian distribution of the probability of the local exchange interaction. The absorption spectrum as a function of energy, $A(E)$, is then readily written as

$$A(e) = \int \frac{P_J(|J|, x)}{\sqrt{2\pi}} \exp \left\{ -\frac{E - (|J| + \Delta E_l)}{2\sigma^2} \right\} d|J| \quad (4)$$

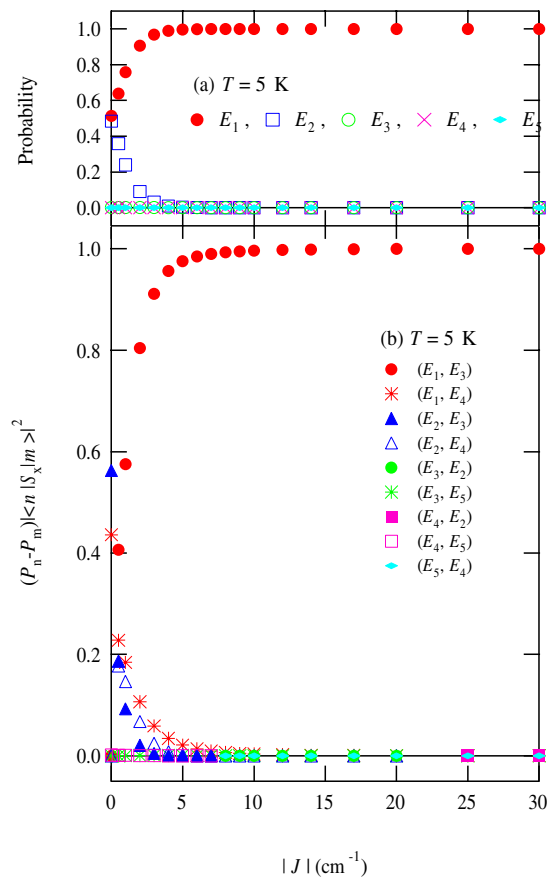


Figure 9. (a) The thermal population of each energy level at $T = 5$ K and (b) the values of $(P_n - P_m)\langle n|S_x|m\rangle^2$ for each transition at $T = 5$ K as a function of $|J|$.

where ΔE_l and the width of the Gaussian distribution, σ , are parameters depending on the iron concentration x . The values for ΔE_l and σ that reproduce the position and the broad shape of the absorption spectrum, respectively, are selected. The concentration dependence of the FIR spectrum of $\text{Fe}_x\text{Zn}_{1-x}\text{F}_2$ calculated using equation (4) is shown in figure 11. These spectra are qualitatively in good agreement with the main signal in the experimental data shown in figure 5. The molecular field approximation does not reproduce exactly the three-peak structure which was suggested from neutron scattering data, but does confirm the basic features of the observed magnetic excitations of $\text{Fe}_x\text{Zn}_{1-x}\text{F}_2$.

The concentration dependences of the parameters ΔE_l and σ are shown in figures 12(a) and (b), respectively. The error bars show the rough tolerance level for each parameter. The ligand field ΔE_l increases slowly with decreasing x , which is consistent with the fact that the value of D obtained from the paramagnetic resonance of Fe^{2+} in ZnF_2 [13] is bigger than that estimated from inelastic neutron scattering data for FeF_2 [14]. The width of the Gaussian distribution, σ , increases quickly with dilution. This growth originates from the randomness increasing with dilution.

Finally, we attempt an assignment to the lower-energy satellite peak that becomes dominant with increasing T . The thermal populations of each energy level at $T = 50$ K are shown

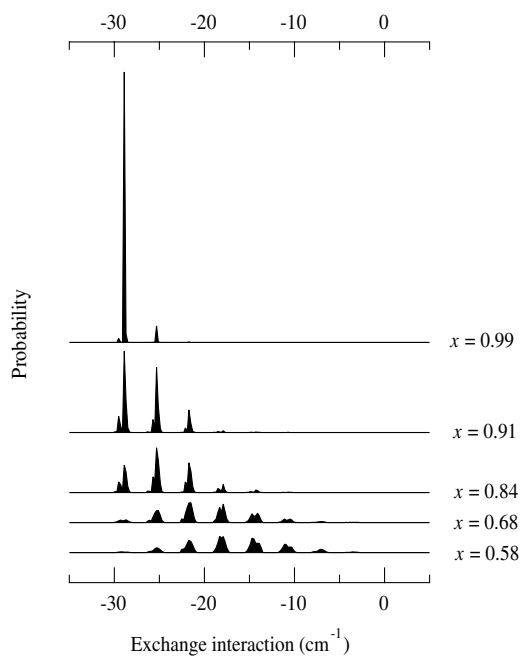


Figure 10. The concentration dependence of the distribution of the local exchange interaction, $P_J(|J|, x)$, in $\text{Fe}_x\text{Zn}_{1-x}\text{F}_2$.

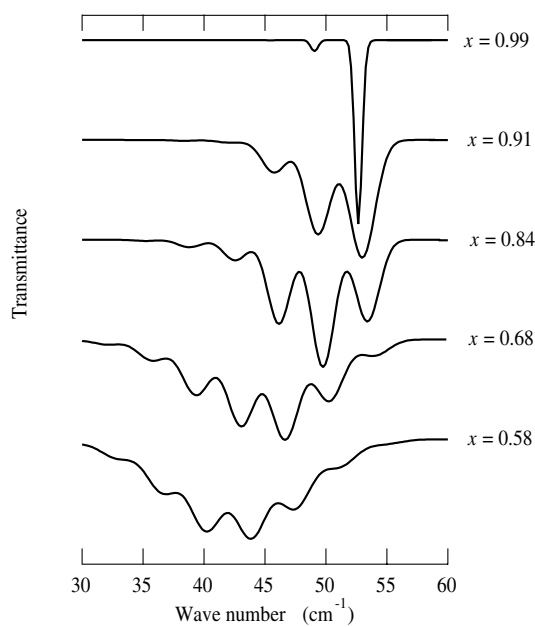


Figure 11. The concentration dependence of the simulated FIR spectrum of $\text{Fe}_x\text{Zn}_{1-x}\text{F}_2$ at low temperature.

in figure 13(a). The probabilities of each of the transitions that can occur at 50 K change with $|J|$ as shown in figure 13(b). From the Mössbauer study, it has been shown that the temperature dependence of the average value of the hyperfine field of $\text{Fe}_{0.69}\text{Zn}_{0.31}\text{F}_2$ [16] coincides with

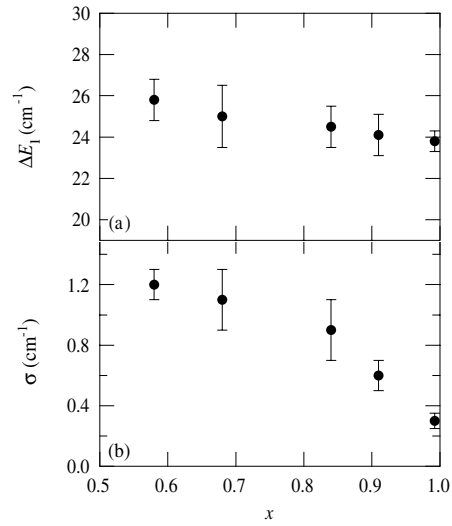


Figure 12. The concentration dependence of (a) the parameter ΔE_l and (b) the width of the Gaussian distribution, σ .

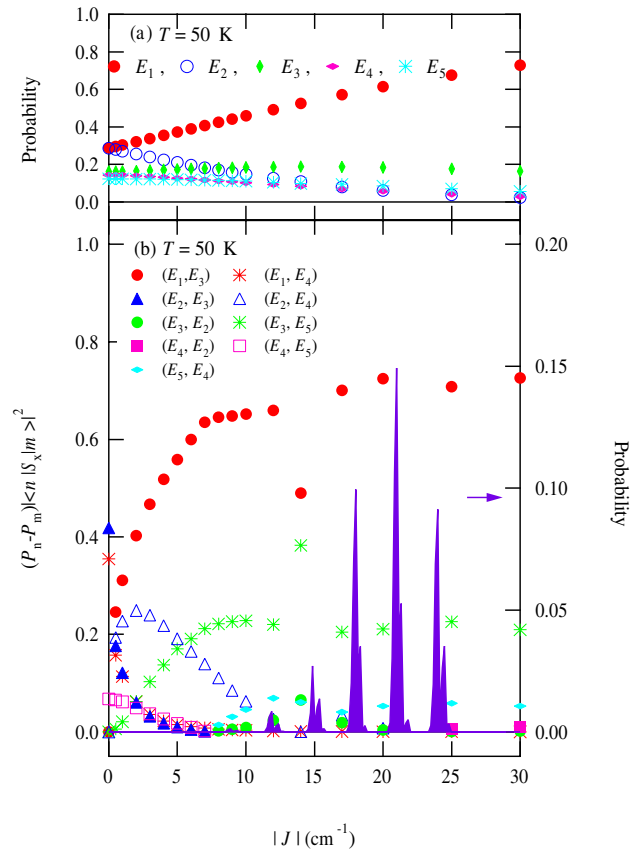


Figure 13. (a) The thermal population of each energy level at $T = 50$ K, and (b) the values of $(P_n - P_m)\langle n|S_x|m\rangle^2$ of each transition at 50 K (left-hand axis), as a function of $|J|$. The purple peaks in (b) show the distribution of the local exchange interaction in $\text{Fe}_{0.84}\text{Zn}_{0.16}\text{F}_2$ at 50 K (right-hand axis).

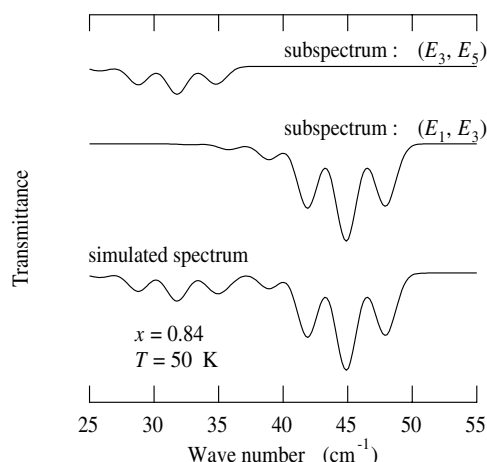


Figure 14. Two subspectra and the simulated FIR spectrum of $\text{Fe}_{0.84}\text{Zn}_{0.16}\text{F}_2$ at $T = 50$ K.

the T -dependence of the hyperfine field of FeF_2 [17] on the reduced scale: the hyperfine axis and the T -axis are normalized by the maximum value and T_N for each sample, respectively. Accordingly, it is reasonable that the T -dependence of the hyperfine field of $\text{Fe}_{0.84}\text{Zn}_{0.16}\text{F}_2$ is also similar to that of FeF_2 on the reduced scale. On the assumption that the T -dependence of the value of each magnetic moment of $\text{Fe}_{0.84}\text{Zn}_{0.16}\text{F}_2$ is of Brillouin type, like that of FeF_2 , the value of the magnetic moment of $\text{Fe}_{0.84}\text{Zn}_{0.16}\text{F}_2$ is, at 50 K, $\sim 83\%$ of its maximum value. In the same way, the probability of the local field of $\text{Fe}_{0.84}\text{Zn}_{0.16}\text{F}_2$ at 50 K is estimated as shown in the figure 13(b), with the right-hand axis. In a region of $|J| = 10\text{--}25$ cm^{-1} in which the local field distribution is operative, there are three transitions with non-zero probability of transition between E_n and E_m with $(n, m) = (1, 3), (3, 5), (5, 4)$. The transition between E_5 and E_4 is not visible in this work, since its energy is below the lower limit of observation. The FIR spectrum of $\text{Fe}_{0.84}\text{Zn}_{0.16}\text{F}_2$ at 50 K is composed of two subspectra that correspond to the transitions between E_n and E_m with $(n, m) = (1, 3), (3, 5)$. With the values of transition probabilities from about 10 to 25 cm^{-1} in figure 13(b), we can estimate that the subspectrum which corresponds to the transition between E_1 and E_3 and the subspectrum which corresponds to the transition between E_3 and E_5 are in a ratio of about 7:2. The transition energy between E_3 and E_5 depends on $|J|$ almost linearly and is lower by approximately 13 cm^{-1} than that between E_1 and E_3 , as shown in figure 7(b). Under the assumptions and with the considerations mentioned above, we analyse the FIR spectrum of $\text{Fe}_{0.84}\text{Zn}_{0.16}\text{F}_2$ at 50 K. We illustrate two subspectra and the simulated FIR spectrum in figure 14. The simulation does not reproduce the experimental spectrum entirely. However, it demonstrates the existence of the low-energy satellite peak. It is suggested that the low-energy satellite peak originates from the transition between two excited states, E_3 and E_5 . This assignment is consistent with the fact that the low-energy satellite peak grows with increasing T .

In conclusion, we have studied the temperature dependence and concentration dependence of the FIR spectra of $\text{Fe}_x\text{Zn}_{1-x}\text{F}_2$. The overall structure of the main peak in each of the low-temperature FIR spectra is reproduced qualitatively by a calculation based on a single-ion excitation model under a molecular field with a distribution of the local exchange interactions. Furthermore, the low-energy satellite peak that grows with increasing temperature is assigned as an excitation from an excited state. The detailed fine structure of the spectra will require further theoretical work beyond the molecular field treatment.

Acknowledgments

The authors would like to thank Dr A Fukaya, Dr T Mutou, and Dr K Hashi for helpful discussions. This work was supported by the MR Science Research Programme of RIKEN and DOE grant No DE-FG03-87ER45324. One of the present authors (JS) was supported by the Special Postdoctoral Researchers Programme of RIKEN and Hayashi memorial foundation for female natural scientists.

References

- [1] Belanger D P 1998 *Spin Glasses and Random Fields* ed A P Young (Singapore: World Scientific) and references therein
- [2] Sykes M F and Essam J W 1964 *Phys. Rev. A* **133** 310
- [3] Stauffer D and Aharony A 1994 *Introduction to Percolation Theory* (London: Taylor and Francis)
- [4] Satooka J and Ito A 1997 *J. Phys. Soc. Japan* **66** 784
- [5] Satooka J and Ito A 1998 *J. Phys.: Condens. Matter* **10** L711
- [6] Paulo H R Barbosa, E P Raposo and Countinho-Filho M D 2001 *Physica A* **295** 140
- [7] Paduani C, Belanger D P, Wang J, Han S-J and Nicklow R M 1994 *Phys. Rev. B* **50** 193
- [8] Ohlman R C and Tinkham M 1961 *Phys. Rev.* **123** 425
- [9] King A R, Jaccarino V, Sakakibara T, Motokawa M and Date M 1981 *Phys. Rev. Lett.* **47** 117
- [10] Stout J W and Reed S A 1954 *J. Am. Chem. Soc.* **76** 5279
- [11] Stout J W and Catalano E 1955 *J. Chem. Phys.* **23** 2013
- [12] Stout J W, Steinfeld M I and Yuzuki M 1968 *J. Appl. Phys.* **39** 1141
- [13] Tinkham M 1956 *Proc. Phys. Soc. A* **236** 535
- [14] Guggenheim H J, Hutchings M T and Rainford B D 1968 *J. Appl. Phys.* **39** 1120
- [15] Hutchings M T, Rainford B D and Guggenheim H J 1970 *J. Phys. C: Solid State Phys.* **3** 307
- [16] Satooka J, Morimoto S and Ito A 1996 *Proc. Conf. ICAME-95* vol 50, p 299
Satooka J 1998 *PhD Thesis* Ochanomizu University
- [17] Wertheim G K and Buchanan D N E 1967 *Phys. Rev.* **161** 478